Chapter 15

Reversible and Reproducible Hydrogen Storage in Single-Walled Carbon Nanotubes Functionalized with Borane

Duraisamy Silambarasan, Velappa Jayaraman Surya, Veerapandy Vasu and Kombiah Iyakutti

Additional information is available at the end of the chapter

http://dx.doi.org/10.5772/intechopen.75763

Abstract

In this chapter, commercial single-walled carbon nanotubes (SWCNTs) were purified by standard methods and functionalized with borane (BH_3). The morphology, presence of elements and vibrations of different functional groups are probed by transmission electron microscopy (TEM), energy dispersive (ED) spectroscopy, and Fourier transform infrared spectroscopy (FTIR), respectively. A Sievert-like hydrogenation setup has been designed and is employed for hydrogenating the functionalized SWCNTs for different time durations. The amount of hydrogen stored in the functionalized SWCNTs has been quantified using elemental analysis, carbon, hydrogen, nitrogen, sulfur (CHNS) combined with thermal (TG/TDS) measurements. A maximum of 4.77 wt.% of hydrogen has been stored at 50°C and the samples become dehydrogenated in the temperature range 90–125°C. From the experiments, it has been found that the amount of hydrogen stored in functionalized SWCNTs increases with increasing hydrogenation duration. Moreover, the entire hydrogenation and dehydrogenation process was examined by Raman, thermal, and elemental analyses together. During the experiments, hydrogenation and dehydrogenation processes were stabilized and were found to be repeatable. Overall, the achieved hydrogen storage capacity of SWCNTS functionalized with BH_3 is close to the US DOE target.

Keywords: single-walled carbon nanotubes, functionalization, borane, density functional theory, hydrogen storage capacity, dehydrogenation

1. Introduction

Hydrogen is evolving as a green fuel for transportation purposes [1, 2]. In recent times, the storage and transport of hydrogen remains a subject of scientific importance. Storage of hydrogen in the form of gas and liquid needs high pressurized environment and cryogenic temperatures which has general problems associated with leakage, safety, and storage capacity. Therefore, storage in solid-state materials provides an appropriate choice. However, the interaction between hydrogen and the host material is either strong (covalent or ionic) or weak (van der Waals forces). For instance, metal hydrides, metal organic frameworks, clathrates, and other nanostructures cannot provide synergic advantages of high gravimetric storage capacity, reliability, and suitable kinetics for applications [3–6]. Carbon-based nanostructures have attracted the scientific community as one of the promising materials for hydrogen storage [7–10]. Among them, carbon nanotubes (CNTs) are widely reported to be potential materials for hydrogen storage [11–17]. CNTs possess unique properties such as hollowness, cylindrical shape, interstitial sites, nanometer scale diameter, and porosity that make them as one of the viable candidates for hydrogen storage [17]. An attempt of hydrogen storage in SWCNT bundles made by Dillon et al. [18] has led to broad investigation on CNTs for hydrogen storage. Further experimentations on hydrogen storage in CNTs indicated that bare CNTs are not suitable material for the storage of hydrogen [19–23]. This is because of the weak interaction (van der Waals interaction) between hydrogen molecules and CNTs; hence, more hydrogen can be stored only at lower temperatures through physisorption. Functionalization of CNTs by the addition of atoms or molecules enhances the interaction between hydrogen and CNTs which results in higher storage capacity [24–29]. Moreover, the functionalization of SWCNTs with transition-metal atoms itself occupies more weight percentage on SWCNTs [30]; and also they form strong metal hydrides while hydrogenation which inturn obviously reduce the space for hydrogen storage [31, 32].

In this chapter, a hydrogen storage medium (HSM) based on SWCNTs, capable of storing and delivering hydrogen in the temperature range suitable for fuel cell applications has been developed. Here, the SWCNTs are modified by means of functionalizing them with BH_3. Our earlier computational studies [27] based on density functional theory (DFT) exhibited that functionalization of SWCNTs with BH_3 increases the binding energy of hydrogen molecules, thereby improving the storage capacity too. The theoretical results inspired us to choose BH_3 for functionalization of SWCNTs, experimentally. Moreover, it was pre-determined to carry out the hydrogenation experiments just above room temperature. This was due to the fact that hydrogen storage at very lower temperature and pressure conditions is not feasible for mobile applications. Hydrogenation of the functionalized SWCNTs has been performed for different time durations. Further, the hydrogenated samples were annealed to check the desorption of hydrogen. The amount of hydrogen uptake and desorption temperature range have been calculated. The binding energy of hydrogen and the nature of hydrogen binding were estimated based on the characterization results. Both hydrogenation and dehydrogenation experiments were repeated to examine the reproducibility.

http://dx.doi.org/10.5772/intechopen.75763

2. Theoretical background

To understand the hydrogen storage behavior of CNT and the mechanism of hydrogen binding, we have investigated the hydrogen storage capacity of CNT (10, 0) functionalized with BH_3 using DFT calculations implemented in VASP (Vienna Ab-initio Simulation Package). **Figure 1** shows the front and top views of CNT (10, 0). CNT (10, 0) is an achiral type of zigzag nanotube, whose mirror image has an identical structure to the original one. The shape of the cross section is trans-type. The radius of the tube is 3.96 Å and it has 20 hexagons and 40 carbon atoms per unit cell.

2.1. Computational details

Ultra-soft pseudopotentials treating the electronic states as valence C: $2s^2\ 2p^2$; B: $2s^2\ p^1$; H: $1s^1$ were used. The local density approximation (LDA) was adopted for the exchange-correlation functional. Two unit cells of (10, 0) were taken in a super cell of geometry $28 \times 28 \times 7.92$ Å. The super cell was taken to be large enough since the periodic repetitions do not lead to any effective interactions between neighboring tubes. The super cell of the tube has 20 half and full hexagons. The energy cutoff for the plane wave basis set was 287 eV. The Brillouin zone was sampled by $1 \times 1 \times 8$ mesh points with Monkhorst-pack *k*-point scheme [33]. Twenty BH_3 molecules were attached on 20 full hexagons around the CNT; this corresponds to the full coverage case. The structures were optimized using conjugate gradient algorithm. Convergence was achieved when the energy was less than 1×10^{-5} eV/atom and 0.5×10^{-5} eV/Å. The hydrogen molecules were attached to the SWCNT–BH_3 complex with a bond length of 0.74 Å parallel to the tube axis. The binding energy of the BH_3 molecule was calculated as

$$E_B\ (BH_3) = [E_T\ (SWCNT - 20BH_3) - E_T\ (SWCNT) - 20E_T\ (BH_3)]/m \quad (1)$$

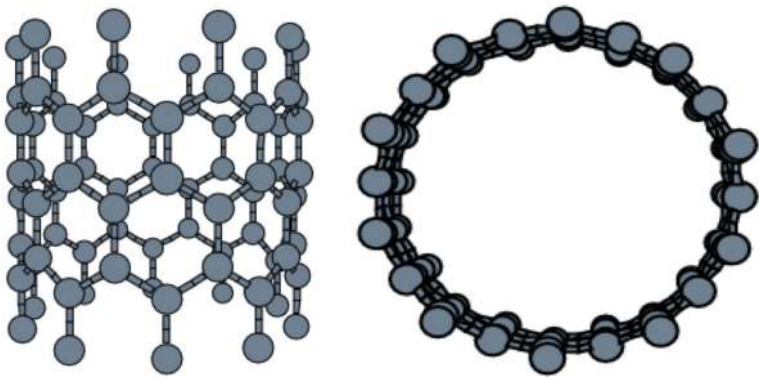

Figure 1. Front and top views of CNT (10, 0).

In a similar way, the binding energy per H_2 molecule was calculated as

$$E_B\,(H_2) = [E_T\,(\mathrm{SWCNT} - 20BH_3 + mH_2) - E_T\,(\mathrm{SWCNT} - 20BH_3) - m \times E_T\,(H_2)]/m \quad (2)$$

where E_T denotes the total energy of the respective systems. The integer m represents the number of H_2 molecule adsorbed on the surface.

2.2. Functionalization

Being light weight and hydrogen rich, BH_3 is able to adsorb H_2 molecules as adsorbates on the surface of CNT. Two unit cells of CNT (10, 0) contain 20 complete hexagons. It is reported that the center of a hexagon is the most stable state for adsorbates [34]. We have attached a single BH_3 on the center of each hexagon at a distance of 2 Å from the surface of the tube. The system $C20BH_3$ refers to CNT (10, 0) + $20BH_3$ complex. After relaxation, the equilibrium position of BH_3 occurs at 2.6 Å from the surface of the tube with an increased bond length of 1.2 Å and an average bond angle of 119°. **Figure 2a** and **b** shows the structure of $C20BH_3$ before and after relaxation, respectively. The binding energy per BH_3 is 3.98 eV. In the figures, gray, parrot green and white color balls represent the carbon, boron, and hydrogen atoms, respectively.

2.3. Hydrogenation

2.3.1. C20(BH_3 + H_2)

A single H_2 molecule is attached to each BH_3 at 2 Å distance from the surface of the tube in the relaxed structure of $C20BH_3$. This complex C20(BH_3 + H_2) is relaxed and the H_2 close to BH_3 has been displaced. Now the distance between BH_3 and H_2 reduces to 1.47 Å. After relaxation, the bond length of H_2 molecule has been increased from 0.74 to 0.9 Å. The relaxed structure of the system C20(BH_3 + H_2) is shown in **Figure 3a**. The binding energy of a single H_2 molecule is 0.86 eV, the storage capacity is 3.16 wt%, and the desorption temperature is 1100 K.

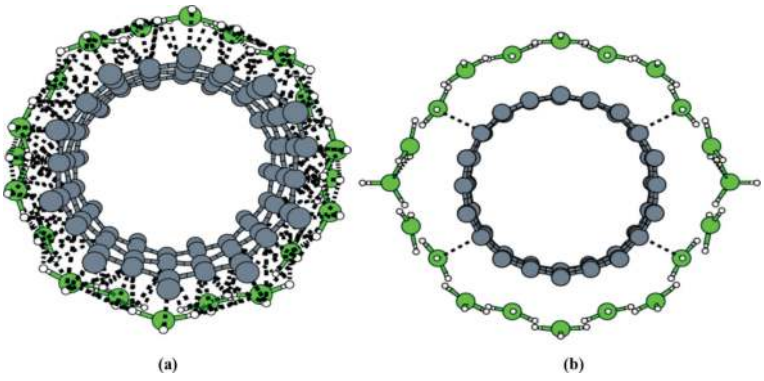

Figure 2. Structure of $C20BH_3$ before relaxation and after relaxation.

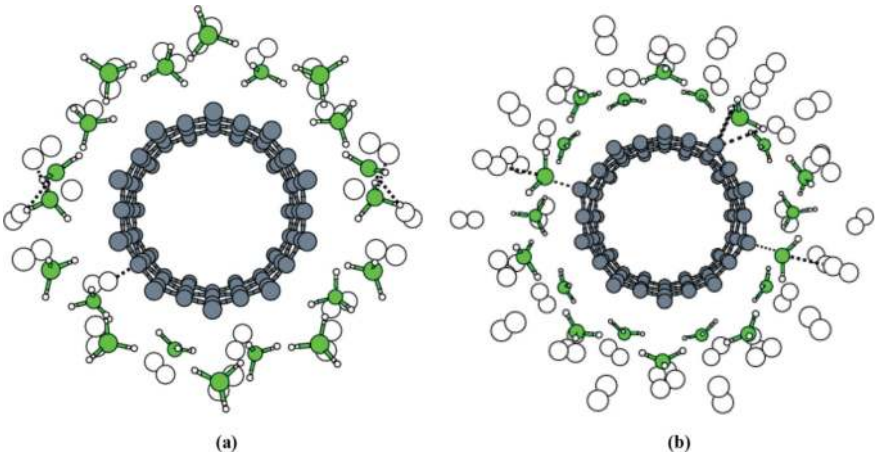

Figure 3. (a) Relaxed structure of C20(BH_3 + H_2) (b) relaxed structure of C20(BH_3 + $2H_2$).

2.3.2. C20(BH_3 + $2H_2$)

Another H_2 molecule is attached to each BH_3. The C20(BH_3 + $2H_2$) structure is relaxed and the H_2 has been displaced from the distance of 2 to 4 Å. After relaxation, the bond length of H_2 molecule has been increased from 0.74 to 0.78 Å. The relaxed structure of the system C20 (BH_3 + $2H_2$) is shown in **Figure 3b**. The binding energy of a H_2 molecule is 0.38 eV, the hydrogen storage capacity is 6.12 wt%, and the desorption temperature is calculated as 486 K.

2.3.3. C20(BH_3 + $3H_2$)

The binding energy of the system C20(BH_3 + $2H_2$) lies in the range of ideal binding energy 0.2–0.4 eV. Hence, the system can adsorb more number of hydrogen. The third H_2 adsorbed on BH_3 is moved away from the BH_3 after relaxation. It is adsorbed at 3.42 Å and the bond length of H_2 molecule has been increased from 0.74 to 0.83 Å. The relaxed structure of the system C20 (BH_3 + $3H_2$) is shown in **Figure 4a**. The binding energy of a H_2 molecule is 0.24 eV, the storage capacity of the system is 8.9 wt%, and the desorption temperature is 307 K.

2.3.4. C20(BH_3 + $4H_2$)

Another H_2 molecule is added to each BH_3. This structure is relaxed and the H_2 has been adsorbed at a distance of 3.39 Å. After relaxation, the bond length of H_2 molecule has been increased from 0.74 to 0.83 Å. The relaxed structure of the system C20(BH_3 + $4H_2$) is shown in **Figure 4b**. In this case, the H_2 molecules are weakly bound, and the binding energy is found to be 0.16 eV, which lies below the ideal binding energy of H_2.

All H_2 are molecularly physisorbed through BH_3 and oriented randomly on CNT. The binding energy of H_2, storage capacity, and desorption temperature of all the systems are given in **Table 1**. The electrostatic interaction is responsible for the binding of H_2 on the (CNT + BH_3)

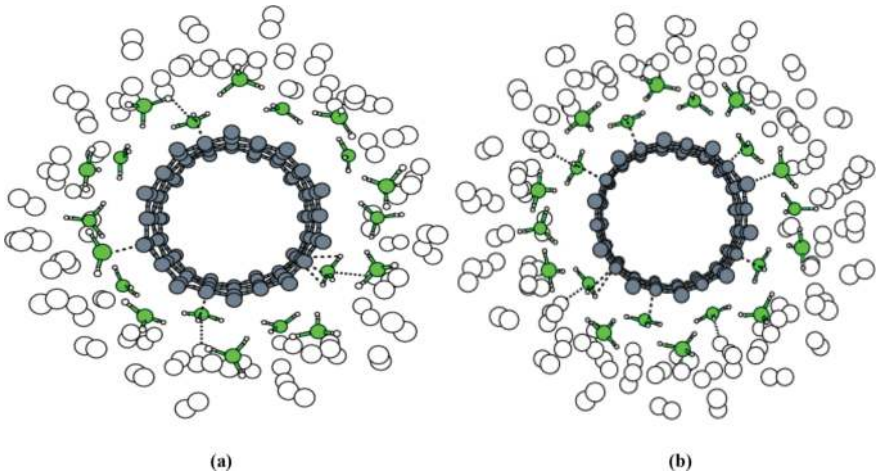

Figure 4. (a) Relaxed structure of C20(BH_3 + $3H_2$) (b) relaxed structure of C20(BH_3 + $4H_2$).

System	Binding energy/H_2 (eV)	Desorption temperature (K)	Storage capacity (wt%)
CNT20(BH_3 + H_2)	0.86	1100	3.16
CNT20(BH_3 + $2H_2$)	0.38	486	6.12
CNT20(BH_3 + $3H_2$)	0.24	307	8.90
CNT20(BH_3 + $4H_2$)	0.16	208	11.5

Table 1. Storage capacities for system C20(BH_3 + nH_2) (n = 1–4).

complex. Since the binding energy of BH_3 is higher than the H_2 binding energy range, only H_2 molecules will be released during desorption and not the BH_3 molecules.

3. Experimental

3.1. Materials

SWCNTs were purchased from Sigma Aldrich with a purity of >98% and purified using acid treatment. $LiBH_4$ was purchased from Sigma Aldrich with an assay of >95%. The other reagents and chemicals used for experiments were purchased from Merck with 99% purity. Alumina substrates of dimension 19 × 19 × 0.65 mm were used. The substrates were cleaned with chromic acid, acetone, and distilled water by means of sonication for 30 minutes (alumina substrates were taken as they are stable at higher temperatures).

3.2. Purification of SWCNTs

Generally, commercial CNTs contain a major component of CNTs along with amorphous carbon structures and metal catalyst impurities (that might be used during the synthesis

process) in few proportions. Hence, it is essential to purify the CNTs before conducting experiments. The purification steps involved heating at 300°C for 1 hour, acid treatment, and repeated washing.

3.3. Designing of hydrogen storage setup

A chamber made up of stainless steel has been designed for our hydrogen storage experiments and is named as hydrogen storage setup. The length of the chamber is about 45 cm with a diameter about 10 cm. The thickness of the stainless sheet is about 0.5 cm. The schematic diagram of the hydrogen storage setup is shown in **Figure 5**. In the figure, the size of the gas inlet valve is large compared to the gas outlet valve. This has been made intentionally to make some amount of gas exist in the chamber to react with samples during the hydrogenation experiment. Moreover, the sample is placed in the path of gas outlet. This is because of the reason that; the gas should meet the sample before leaving the chamber. The sample holder is also made up of stainless steel sheet. Commercial hydrogen gas (purity >90%) cylinders has been used for the experiments.

3.4. SWCNT deposition and functionalization

A well dispersed solution of SWCNTs was deposited on alumina substrates and a subsequent heating up to 200°C was done. $LiBH_4$ (the precursor for BH_3) was mixed with diethyl ether ($(C_2H_5)_2O$) in a ratio of 25 mg/ml, and it was drop casted over the surface of SWCNTs. Then the substrates were heated to 275°C (decomposition temperature of $LiBH_4$) for 1 hour, which yields borane. The released BH_3 reacts with SWCNTs and forms a complex, SWCNT + BH_3. This complex acts as an HSM.

3.5. Hydrogenation

The functionalized samples were loaded in the hydrogenation setup and hydrogenated as detailed in this section. Initially, we would like to know whether the functionalized SWCNTs exhibit hydrogen storage capability at a temperature around 100 or 50°C. For that, the functionalized samples were maintained at a particular temperature and the hydrogen gas was allowed to flow for some time interval at a known flow rate and then the samples were left in the chamber to attain room temperature. After hydrogenation, the hydrogen content present in the samples was again estimated using CHNS-elemental analysis. The initial hydrogenation results we got were encouraging. The results are presented in **Table 2**. After the confirmation of the hydrogen storage ability of functionalized SWCNTs, we improved our hydrogenation setup by introducing a few controlled valves to reduce the leakage of hydrogen gas. The

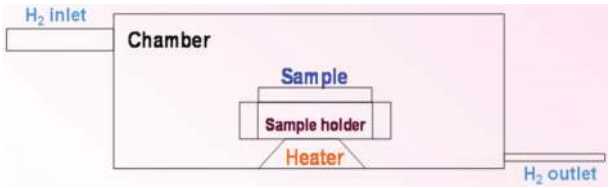

Figure 5. Schematic diagram of hydrogen storage setup.

Substrate temperature (°C)	Flow rate (liter/min)	Flow duration (min)	Storage capacity (wt.%)
100	1	4	0.68
100	1	20	0.87
50	3	20	1.50

Table 2. Initial hydrogenation results.

Sample index	Flow rate (liter/min)	Flow duration (min)	Storage capacity (wt.%)
CBH1	0.5	30	3.27
CBH2	0.5	35	3.78
CBH3	0.5	40	4.35
CBH4	0.5	45	4.77

CBH1–4 represents four different hydrogenated samples.

Table 3. Optimized hydrogenation results.

functionalized samples were loaded in the hydrogenation setup and hydrogenated for different time durations by maintaining the substrate temperature at 50°C and the hydrogen flow rate at ~0.5 liter/minute. The storage capacities were calculated as the difference of hydrogen content in the samples before and after the hydrogenation experiment and the results are presented in **Table 3**.

3.6. Dehydrogenation

Thermal annealing was used to stimulate the dehydrogenation from the hydrogenated samples. The hydrogenated samples were annealed at 200°C for 1 hour. The temperature was controlled by a digital proportional-integral-derivative (PID) controller. After annealing, the samples were left in the furnace to reach room temperature and then characterized.

3.7. Characterizations

The morphology of SWCNTs was analyzed by transmission electron microscope (TEM) imaging using a JEOL JEM 2100 model unit with an accelerating voltage of 200 kV. The energy dispersive (ED) spectrum of SWCNTs was recorded using the JEOL model 6390 unit with an accelerating voltage of 5 kV. Infrared (IR) spectrum was recorded over the range 4000–450 cm^{-1} using a Shimadzu model (FTIR-8400S, CE) spectrometer at room temperature with a resolution of 1 cm^{-1}. X-ray photoelectron spectroscopy (XPS) measurements were taken using a Scienta ESCA3000 model spectrometer. Raman measurements were carried out using a Labram HR800 model spectrometer. The samples were excited with a 17 mW (~633 nm) He–Ne laser. Before taking measurements, the spectrometer was calibrated using a silica wafer. An Elementar Vario EL III model analyzer was used for CHNS-elemental analysis. A Perkin Elmer-Diamond model unit was used to study the thermal response of the samples.

http://dx.doi.org/10.5772/intechopen.75763

4. Results and discussion

4.1. Morphology, elemental and functional group analyses

Figure 6(a) shows the TEM image of SWCNTs. The image reveals the good distribution and separation of SWCNTs with an average diameter of 2–4 nm. The ED spectrum of SWCNTs shown in **Figure 6(b)** displays the existence of carbon and oxygen in the sample along with copper resulting from the supporting grid. The functional groups present in the functionalized SWCNTs are determined from the bands appearing in the IR spectrum. **Figure 7** shows the IR spectrum of the functionalized SWCNTs. Absorption peaks at 1608, 1027, and 729 cm^{-1} correspond to C=C stretching, C–C stretching, and skeleton vibrations of carbon atoms in CNTs, respectively. The electrostatic interaction between BH_3 and CNT caused the deformation [35] and asymmetric stretching [36] of B–H bonds; the resultant respective peaks are observed at 1260 and 2350 cm^{-1}. On the other hand, the appearance of a peak at 1430 cm^{-1} is due to C–H asymmetric deformation vibrations of the dissociative adsorption of BH_3 on CNT. The results of the IR study authenticate that the SWCNTs functionalized with BH_3 is stable and is agreed with the theoretical results [25].

The composition of elements present in the functionalized sample is found from the X-ray photoelectron spectroscopy (XPS) spectrum. The full survey spectrum of the functionalized sample is shown in **Figure 8**. The de-convoluted XPS spectra of the individual components, such as C, Li, B, and O are shown in **Figure 9(a)–(d)**, respectively. The C 1s component at 286.3 eV is assigned to C–O or C–OH bond [37] and a small peak at 290.9 eV is due to Li_2CO_3. The peak at 56.7 eV is attributed to Li. The lower binding energy component (188.9 eV) is assigned to boron atoms bonded only to the other boron atoms [38, 39], whereas the higher energy component (193.8 eV) represents the oxidized boron [40, 41]. The main O 1s component is assigned to boron oxide [39]. The weight percentages are 44.7, 15.4, 7.1, and 28.7 for the elements C, B, Li, and O, respectively. From the XPS studies, it is observed that the incorporation of

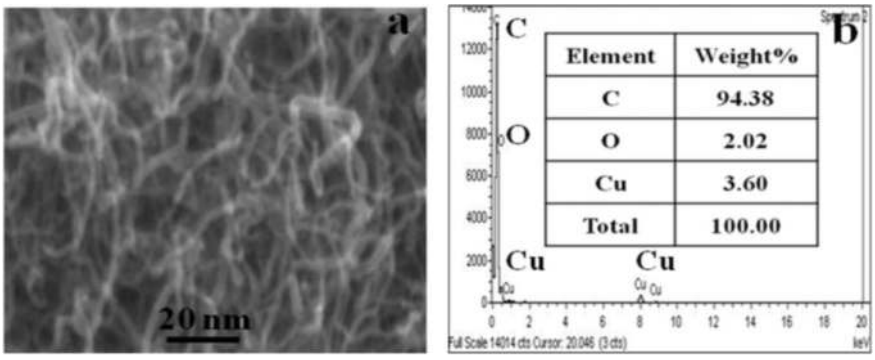

(a) (b)

Figure 6. (a) TEM image and (b) ED spectrum of SWCNTs.

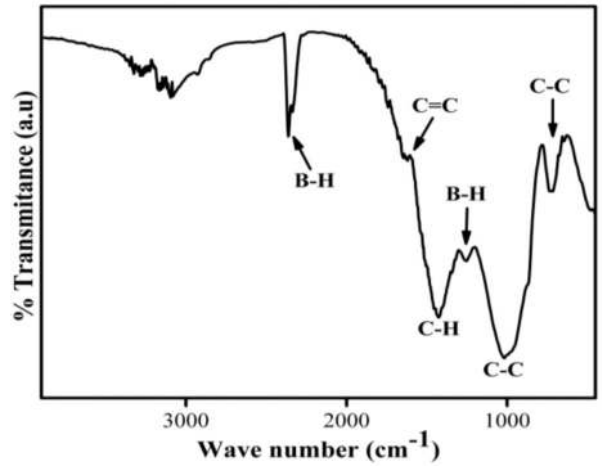

Figure 7. IR spectrum of functionalized SWCNTs.

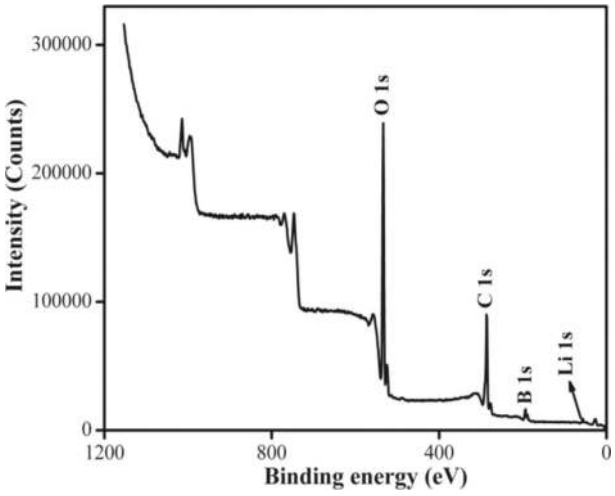

Figure 8. XPS survey spectrum of functionalized SWCNTs.

oxygen present in the functionalized sample is ~30 wt%. This incorporation may be due to the deposition of samples carried out in open atmosphere.

4.2. Hydrogenation analyses

The quantity of hydrogen stored in the functionalized samples is measured from the CHNS-elemental analysis. The hydrogenation results are shown in **Tables 2** and **3**. The storage capacity at this temperature (50°C) of the designed storage medium is much higher than the

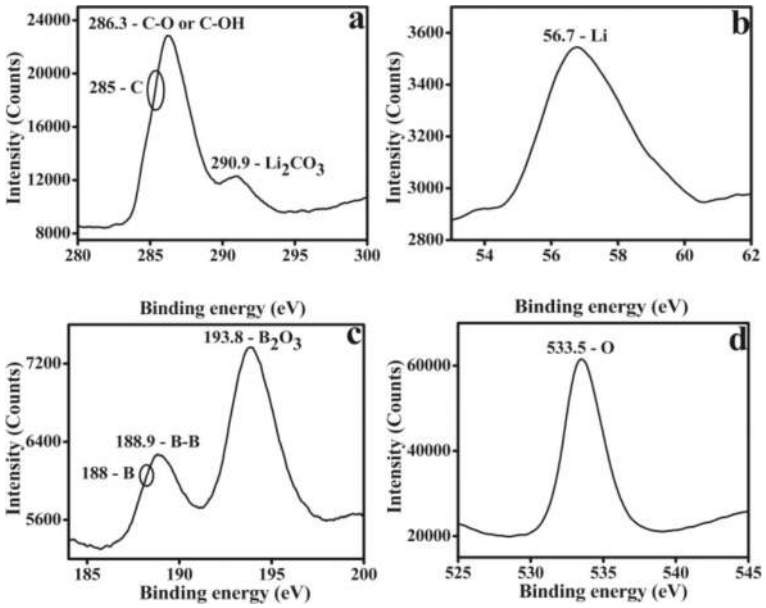

Figure 9. De-convoluted XPS spectra of (a) carbon, (b) Lithium, (c) boron and (d) oxygen.

values reported by Ioannatos et al. [1], Im et al. [39], and Li et al. [42]. **Figure 10** shows the Raman spectra of SWCNTs (C), SWCNTs functionalized with BH_3 (CB), and hydrogenated functionalized SWCNTs (CBH). In the entire spectrum, the D and G bands appeared around 1350 and 1570 cm^{-1}, respectively. The defect concentration in CNT can be measured by calculating the intensity ratio of the D to G band. As the defect density increased for the samples from SWCNTs, functionalized SWCNTs to hydrogenated SWCNTs, the corresponding D/G ratio has also increased from 0.08, 0.21, to 0.59. The Raman and CHN-elemental analyses are together used to probe dehydrogenation (the dehydrogenated sample and is designated as DCB). The hydrogenation and dehydrogenation experiments are repeated a number of times and the corresponding D/G ratio is also measured. The deterioration level of the functionalized SWCNTs after repeated hydrogenation and dehydrogenation is only about 2.3%. A similar change of 3% was reported by Zhang et al. [43]. The hydrogen storage capacity varies 5% about the mean value.

4.3. Desorption analyses

Figure 11 shows the TG spectra of all hydrogenated samples CBH1, CBH2, CBH3, CBH4 and **Figure 12** shows the region associated with hydrogen desorption. The spectrum for the sample CBH1 shows a weight loss of about 3.27 wt% in the temperature range 105–140°C and it corresponds to the desorption of stored hydrogen from the sample. The desorption profile shown in **Figure 12** exactly measures the starting and end temperatures of the desorption. The primary weight loss is attributed to hydrogen desorption since the desorption of borane starts above 275°C. The findings obtained from TG analysis are in line with Raman results.

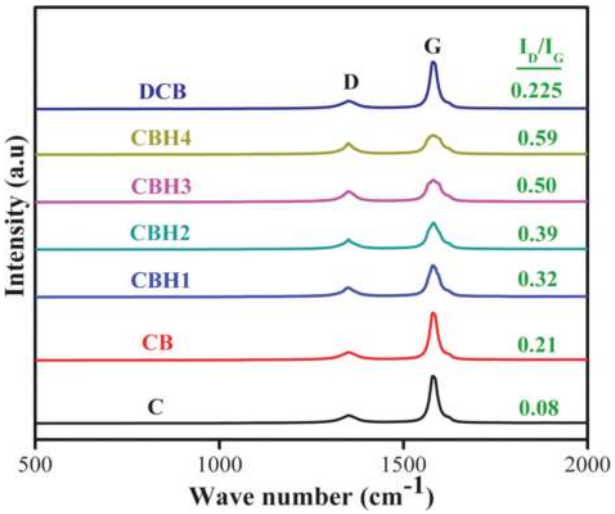

Figure 10. Raman spectra of all the samples.

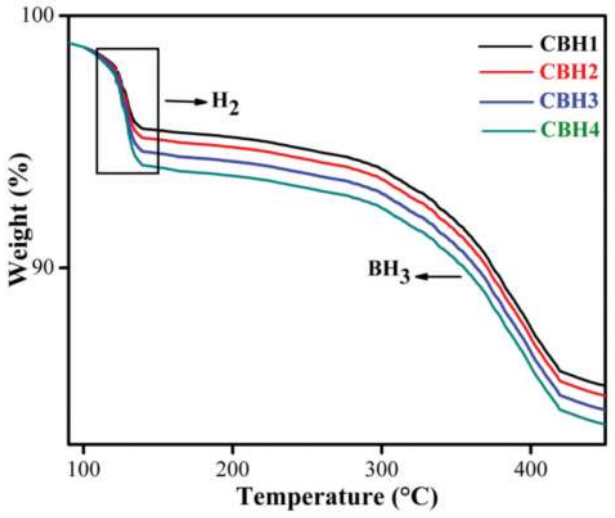

Figure 11. TG spectra of all the hydrogenated samples.

The activation energy of desorption, E_d can be calculated from the maximum desorption peak using the following Equation [1],

$$\ln\left(T_m{}^2/\beta\right) = E_d/R{*}T_m \tag{3}$$

where T_m is the temperature at maximum peak (121°C), β is the heating rate (10°C/min), and R is the universal gas constant. The calculated activation energy of desorption for the sample

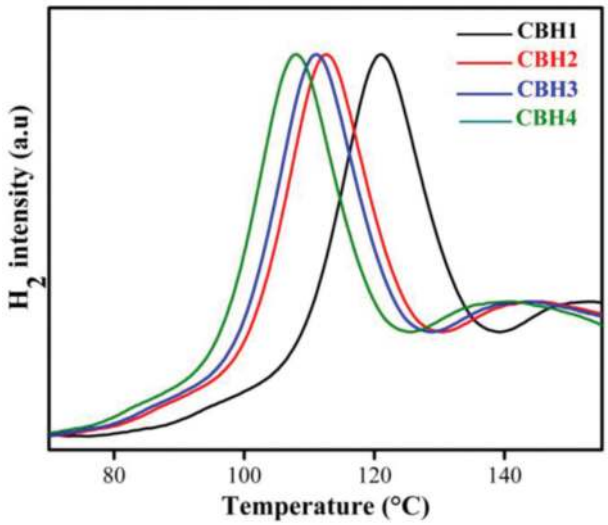

Figure 12. Desorption spectra of all the hydrogenated samples.

Sample index	H_2 (wt.%)	T_m (°C)	E_d (kJ/mol)	E_B (eV)
CBH1	3.277	121	20.66	0.310
CBH2	3.785	113	20.11	0.302
CBH3	4.345	111	19.97	0.300
CBH4	4.770	107	19.69	0.287

Table 4. Hydrogen desorption characteristic parameters.

CBH1 is 20.66 kJ/mol. Van't Hoff Equation [2] is applied to estimate the binding energy (E_B) of hydrogen,

$$E_B = T * K_B\ (\Delta S/R) \tag{4}$$

where T is the desorption temperature, K_B is Boltzmann's constant and ΔS is change in entropy. The estimated binding energy value is 0.31 eV per H_2 for the temperature 121°C. The various factors found from the hydrogenation and dehydrogenation studies are presented in **Table 4**. From the desorption profile, it is apparent that the desorption peak temperature reduces with the increase in hydrogen storage capacity.

The obtained binding energy values fall in the weak chemisorption region, and is in the suggested region (0.2–0.4 eV) for a practical hydrogen storage medium [7]. The functionalized SWCNTs and hydrogen interact through a combination of inductive, covalent, and electrostatic charge transfer mechanisms [7, 25] amidst CNTs and hydrogen, borane anchored as a bridge. The composition presence of hydrogen measured from CHNS analysis is equivalent to

the weight lost in the thermogravimetric study, i.e., the quantity of hydrogen desorbed is equal to the quantity of hydrogen adsorbed. Thus, our system exhibits 100% desorption in the temperature range 90–140°C, which may be more suitable for vehicular-based fuel cells than the desorption temperature reported by Arellano et al. [21] and Lee et al. [44]. This observation reveals that the adsorption sites on CNTs surface are relatively uniform and that there are no sites which form very weak or very strong adsorption bonds [1]. On the whole, the present investigation reveals the ability of reversible hydrogen uptake by the functionalized SWCNTs.

5. Summary

In this chapter, the hydrogenation and dehydrogenation studies of SWCNTs functionalized with BH_3 are presented. The SWCNTs are successfully functionalized with BH_3 using $LiBH_4$ as the precursor. The deposition process involves a simple drop casting method. The presence of BH_3 in the functionalized sample is confirmed using IR study. From XPS study, apart from C, the presence of Li, B, and O are also observed in the functionalized sample. Then, the functionalized samples are hydrogenated for different time durations. A maximum storage capacity of 4.77 wt% is achieved at 50°C, which is close to the U.S. DOE target of 5.5 wt% for an HSM to be used for on-board applications. Based on thermal annealing, a systematic investigation of desorption of hydrogen is carried out. The evidences for desorption is provided by Raman, CHNS-elemental, and TG measurements. The results show that thermal annealing treatment induces desorption of hydrogen from the hydrogenated functionalized SWCNTs. The stored hydrogen is released over the temperature range 90–140°C. The deterioration level of the sample is also checked using Raman analysis. Overall, this investigation shows that the SWCNTs functionalized with BH_3 may be a suitable reversible hydrogen storage system that is capable of storing and releasing hydrogen under optimum conditions over repeated cycles suitable for hydrogen-based fuel cells used in vehicular applications.

Author details

Duraisamy Silambarasan[1,2]*, Velappa Jayaraman Surya[3,4], Veerapandy Vasu[1] and Kombiah Iyakutti[3]

*Address all correspondence to: simbuphysics@yahoo.com

1 School of Physics, Madurai Kamaraj University, Madurai, Tamil Nadu, India

2 PG and Research Department of Physics, The MDT Hindu College, Tirunelveli, Tamil Nadu, India

3 Department of Physics and Nanotechnology, SRM University, Kattankulathur, Tamil Nadu, India

4 SRM Research Institute, SRM University, Kattankulathur, Tamil Nadu, India

References

[1] Ioannatos GE, Verykios XE. H_2 storage on single- and multi-walled carbon nanotubes. International Journal of Hydrogen Energy. 2010;**35**:622-628. DOI: 10.1016/j.ijhydene.2009.11.029

[2] Durgun E, Ciraci S, Yildirim T. Functionalization of carbon-based nanostructures with light transition-metal atoms for hydrogen storage. Physical Review B. 2008;**77**:085405-085409. DOI: 10.1103/PhysRevB.77.085405

[3] Orimo S, Nakamori Y, Eliseo JR, Züttel A, Jensen CM. Complex Hydrides for Hydrogen Storage. Chemical Review. 2007;**107**:4111-4132. DOI: 10.1021/cr0501846

[4] Zhang J, Hu YH. Intermediate species and kinetics of lithium imide decomposition. International Journal of Hydrogen Energy. 2012;**37**:10467-10472. DOI: 10.1016/j.ijhydene.2011.12.061

[5] Hu YH, Zhang L. Hydrogen storage in metal-organic frameworks. Advanced Materials. 2010;**22**:E117-E130. DOI: 10.1002/adma.200902096

[6] Murray LJ, Dinca M, Long JR. Hydrogen storage in metal-organic frameworks. Chemical Society Review. 2009;**38**:1294-1314. DOI: 10.1039/B802256A

[7] Lochan RC, Head-Gordon M. Computational studies of molecular hydrogen binding affinities: The role of dispersion forces, electrostatics, and orbital interactions. Physical Chemistry Chemical Physics. 2006;**8**:1357-1370. DOI: 10.1039/b515409j

[8] Li J, Terumi F, Hajime G, Toshiyuki O, Yoshiya F, Sidney Y. Theoretical evaluation of hydrogen storage capacity in pure carbon nanostructures. Journal of Chemical Physics. 2003;**119**:2376-2385. DOI: 10.1063/1.1582831

[9] Duplock EJ, Scheffler M, Lindan PJD. Hallmark of perfect graphene. Physical Review Letters. 2004;**92**:225502–1–225502-4. DOI: 10.1103/PhysRevLett.92.225502

[10] Zuttel A, Sudan P, Mauron P, Kyobayashi T, Emenenrgger C, Schlapbach L. Hydrogen storage in carbon nanostructures. International Journal of Hydrogen Energy. 2002;**27**: 203-212. DOI : S0360-3199(01)00108-2

[11] Zhao M-W, Xia Y-Y, Ma Y-C, Ying M-J, Liu X-D, Mei L-M. Tunable adsorption and desorption of hydrogen atoms on single-walled carbon nanotubes. Chinese Physics Letters. 2002;**19**:1498-1500. DOI: cpl.iphy.ac.cn/Y2002/V19/I10/01498

[12] Okati A, Zolfaghari A, Hashemi FS, Anousheh N, Jooya H. Hydrogen Physisorption on stone-Wales defect-embedded single-walled carbon nanotubes. Fullerenes, Nanotubes, and Carbon Nanostructures. 2009;**17**:324-335. DOI: 10.1080/15363830902776599

[13] Muniz AR, Meyyappan M, Maroudas D. Effects of hydrogen chemisorption on the structure and deformation of single-walled carbon nanotubes. Applied Physics Letters. 2009;**95**:163111–1–163111-3. DOI: 10.1063/1.3095923

[14] Rzepka M, Lamp P, de la Casa-Lillo MA. Physisorption of hydrogen on microporous carbon and carbon nanotubes. The Journal of Physical Chemistry. B 1998;**102**:10894-10898. DOI:10.1021/jp9829602

[15] Lee SM, An KH, Lee YH, Seifert G, Frauenheim T. A hydrogen storage mechanism in single-walled carbon nanotubes. Journal of American Chemical Society. 2001;**123**:5059-5063. DOI: 10.1021/ja003751+

[16] Darkrim FL, Levesque D. Monte Carlo simulations of hydrogen adsorption in single-walled carbon nanotubes. Journal of Chemical Physics. 1998;**109**:4981-4984. DOI: 10.1063/1.477109

[17] Cheng JR, Yuan XH, Zhao L, Huang DC, Zhao M, Dai L, Ding R. GCMC simulation of hydrogen physisorption on carbon nanotubes and nanotube arrays. Carbon. 2004;**42**:2019-2024. DOI: 10.1016/j.carbon.2004.04.006

[18] He Z, Wang S, Wang X, Iqbal Z. Hydrogen storage in hierarchical nanoporous silicon–carbon nanotube architectures. International Journal of Energy Research. 2013;**37**:754-760. DOI: 10.1002/er.2979

[19] Dillon AC, Jones KM, Bekkendahl TA, Kiang CH, Bethune DS, Heben MJ. Storage of hydrogen in single-walled carbon nanotubes. Nature. 1997;**386**:377-379. DOI: 10.1038/386377a0

[20] Ye Y, Ahn CC, Witham C, Fultz B, Liu J, Rinzler AG, Colbert D, Smith KA, Smalley RE. Hydrogen adsorption and cohesive energy of single-walled carbon nanotubes. Applied Physics Letters. 1999;**74**:2307-2309. DOI: 10.1063/1.123833

[21] Arellano JS, Molina LM, Rubio A, MJ L'p, Alonso JA. Interaction of molecular and atomic hydrogen with (5,5) and (6,6) single-wall carbon nanotubes. Journal of Chemistry Physics. 2002;**117**:2281-2288. DOI: 10.1063/1.1488595

[22] Sudan P, Zuttel A, Mauron P, Emmenegger C, Wenger P, Schlapbach L. Physisorption of hydrogen in single-walled carbon nanotubes. Carbon. 2003;**41**:2377-2383. DOI: 10.1016/S0008-6223(03)00290-2

[23] Tibbetts GG, Meisner GP, Olk CH. Hydrogen storage capacity of carbon nanotubes, filaments, and vapor-grown fibers. Carbon. 2001;**39**:2291-2301. DOI: 10.1016/S0008-6223(01)00051-3

[24] Wu XM, Wang Y, Dong KM, Zhou JM, Lin GD, Zhang HB. Study of storage and adsorption/desorption characteristics of H_2 on MWCNTs modified by metal potassium. Acta Chimica Sinica. 2005;**63**:484-490

[25] Surya VJ, Iyakutti K, Rajarajeswari M, Kawazoe Y. Functionalization of single-walled carbon nanotube with borane for hydrogen storage. Physica E: Low-dimensional Systems and Nanostructures. 2009;**41**:1340-1346. DOI: 10.1016/j.physe.2009.03.007

[26] Liu W, Zhao YH, Li Y, Jiang Q, Lavernia EJ. Enhanced hydrogen storage on Li-dispersed carbon nanotubes. Journal of Physical Chemistry C. 2009;**113**:2028-2033. DOI: 10.1021/jp8091418

[27] Surya VJ, Iyakutti K, Venkataramanan NS, Mizuseki H, Kawazoe Y. Single walled carbon nanotubes functionalized with hydrides as potential hydrogen storage media: A survey of intermolecular interactions. Physical Status Solidi B. 2011;**248**:2147-2158. DOI: 10.1002/pssb.201046532

[28] Reyhani A, Mortazavi SZ, Mirershadi S, Moshfegh AZ, Parvin P, Nozad Golikand A. Hydrogen storage in decorated multiwalled carbon nanotubes by Ca, co, Fe, Ni, and Pd nanoparticles under ambient conditions. Journal of Physical Chemistry C. 2011;**115**:6994-7001. DOI: 10.1021/jp108797p

[29] Reddy ALM, Ramaprabhu S. Hydrogen adsorption properties of single-walled carbon nanotube-Nanocrystalline platinum composites. International Journal of Hydrogen Energy. 2008;**33**:1028-1034. DOI: 10.1016/j.ijhydene.2007.11.005

[30] Iyakutti K, Kawazoe Y, Rajarajeswari M, Surya VJ. Aluminum hydride coated single-walled carbon nanotube as a hydrogen storage medium. International Journal of Hydrogen Energy. 2009;**34**:370-375. DOI: 10.1016/j.ijhydene.2008.09.086

[31] Yildirim T, Ciraci S. Titanium-decorated carbon nanotubes as a potential high-capacity hydrogen storage medium. Physical Review Letters. 2005;**94**:175501-1-175501-4. DOI: 10.1103/PhysRevLett.94.175501

[32] Jianwei R, Shijun L, Junmin L. Hydrogen storage of multiwalled carbon nanotubes coated with Pd-Ni nanoparticles under moderate conditions. Chinese Science Bullettin. 2006;**51**: 2959-2963. DOI: 10.1007/s11434-006-2216-8

[33] Monkhorst HJ, Pack JD. Special points for Brillouin-zone integrations. Physical Review B. 1976;**13**:5188-5192

[34] Iyakutti K, Rajarajeswari M, Dharmawardhana MWC. The interaction of nitrogen molecules with (4,0) single-walled carbon nanotube: Electronic and structural effects. Nanotechnology 2008;**19**:185704–185701–185704-4. DOI:10.1088/0957-4484/19/18/185704

[35] Kaldor A, Porter RF. Infrared spectra of the pyrolysis products of Borane carbonyl in an argon matrix. Journal of American Chemical Society. 1971;**93**:2140-2145

[36] Nakamoto K. Infrared and Raman Spectra of Inorganic and Coordination Compounds: Part A: Theory and Applications in Inorganic Chemistry. 6th ed. Newyork: Wiley; 1978. DOI: 10.1002/9780470405840

[37] Vickerman JC. Surface Analysis - The Principle Techniques. 2nd ed. Chichester: Wiley; 1997. DOI: 10.1002/9780470721582

[38] Guo L, Singh RN, Kleebe HJ. Growth of boron-rich nanowires by chemical vapor deposition (CVD). Journal of Nanomaterials. 2006;**2006**:58237-1-58237-6. DOI: 10.1155/JNM/2006/58237

[39] Ong CW, Huang H, Zheng B, Kwok RMW, Hui YY, Lau WM. X-ray photoemission spectroscopy of nonmetallic materials: Electronic structures of boron and BxOy. Journal of Applied Physics. 2004;**95**:3527-3534. DOI: 10.1063/1.1651321

[40] Xu TT, Zheng JG, Wu NQ, Nicholls AW, Roth JR, Dikin DA, Ruoff RS. Crystalline boron Nanoribbons: Synthesis and characterization. Nano Letters. 2004;**4**:963-968. DOI: 10.1021/nl0498785

[41] Im JS, Yun J, Kang SC, Lee JK, Lee Y-S. Hydrogen adsorption on activated carbon nanotubes with an atomic-sized vanadium catalyst investigated by electrical resistance measurements. Applied Surface Science. 2012;**258**:2749-2756. DOI: 10.1016/j.apsusc.2011.10.126

[42] Li B, Huang X, Gong R, Ma M, Yang X, Liang L, Tan B. Catalyzed hydrogen spillover for hydrogen storage on microporous organic polymers. International Journal of Hydrogen Energy. 2012;**37**:12813-12820. DOI: 10.1016/j.ijhydene.2012.05.106

[43] Zhang G, Qi P, Wang X, Lu Y, Mann D, Li H, Dai H. Hydrogenation and Hydrocarbonation and etching of single-walled carbon nanotubes. Journal of American Chemical Society. 2006;**128**:6026-6027. DOI: 10.1021/ja061324b

[44] Lee H, Nguyen MC, Ihm J. Titanium-functional group complexes for high-capacity hydrogen storage materials. Solid State Communication. 2008;**146**:431-434. DOI: 10.1016/j.ssc.2008.03.018